ON RADAR IMAGING OF OCEAN PHENOMENA

V. Kudryavtsev[1,2], D. Akimov[3], J.A. Johannessen[2], O.M. Johannessen[2] and B. Chapron[4]

[1] *Marine Hydrophysical Institute, Sebasopol, Ukraine*
[2] *Nansen Environmental and Remote Sensing Center, Bergen, Norway*
[3] *Nansen International Environmental and Remote Sensing Center, St.Petersburg, Russia*
[4] *Institute Francais de Recherche pour l'Exploitation de la Mer, Plouzane, France*

ABSTRACT

A model of radar imaging of ocean phenomena is proposed. This model is an extension of the background NRCS model [7] in the case of non-uniform medium. Radar scattering component takes into account Bragg and non-Bragg (specular reflections and the impact of wave breaking) scattering mechanisms. Varying surface current, surface temperature (stability effects), and surfactants are the main sources of medium non-uniformities. Transformation of wave spectrum and wave breaking in non-uniform medium is described in the relaxation approximation. Model calculations are compared with field observations. An overall good agreement is obtained. It is shown that wave breaking play important role in the formation of radar signatures of ocean phenomena.

1. INTRODUCTION

Radar signatures of the ocean phenomena (currents features, eddies, temperature fronts, bottom topography, internal waves) have been observed and documented in numerous experiments (e.g. [1, 4, 5, 12]). Experiments showed that radar visibility of ocean phenomena significantly depends on wind conditions, geometry of the radar observations and maybe other poorly studied factors. Wave-current interactions, suppression of waves by surfactants, and influence of atmospheric stratification are the commonly accepted mechanisms responsible for the surface manifestation of the ocean phenomena.

In the present study we propose a radar imaging model which is an extension of the background model [7] in the case of non-uniform medium. In [7] statistical properties of the sea surface results from solution of the energy balance equation. In the extended model the same equations are used to describe evolution of wind waves in a non-uniform medium. This model takes into account radar scattering from breaking waves. Unlike previous studies, the same wave breaking statistics (originally proposed in [10]) is used in both wind waves and radiowave scattering models. It gives a consistency between the components of the radar imaging model. In [8] the background model was applied for the radar modulation transfer function (MTF). It was shown that inclusion of wave breaking significantly improved agreement between theory and measurements. Here (without any additional tuning) we expand the background model [7] to the problem of radar imaging of ocean phenomena.

2. RADAR SCATTERING FROM SEA SURFACE

Following [7] the sea surface is represented as a "regular" (non-breaking) wavy surface sprinkled with a number of breaking zones. Wave breaking provides a strong radar return forming a spike-like structure of radar images. Though the fraction of the sea surface q covered by breaking waves is small, they may significantly contribute to the normalized radar cross section (NRCS). It is suggested that radar returns from the regular surface (its fraction is $(1-q)$) is supported by Bragg scattering (σ_{br}^{p}) and specular reflection (σ_{sp}) from steep surface slopes. Thus the total NRCS is

$$\sigma_0^p = (\sigma_{br}^p + \sigma_{sp})(1-q) + \sigma_{0wb} q \qquad (1)$$

where σ_{0wb} is the NRCS of an individual breaking zone. The quantity q is defined in [7] as a fraction of the sea surface covered by enhanced surface roughness generated by breaking waves, with wavelengths exceeding the radar wavelength by at least a factor of 10. Correspondingly the expression for σ_{0wb} is a consequence of mechanism of specular reflection from breaking zones (see [7], their eq. (55) and (60)). If the impact of breaking waves is ignored, the two first terms in (1) represent composite radar scattering model derived from physical arguments in [14], and later - in [13]. In the composite model spectrum of the sea surface is divided into small scale waves $k > k_d$ (with elevation variance h_S^2) and large scale waves $k < k_d$.

The dividing wavenumber k_d is proportional to radar wavenumber k_r: $k_d = d \cdot k_r$, where d is a constant. In our model dividing parameter is defined as $d = 1/4$, close to the recommendation of [13]. Small-scale waves provide resonant radiowave scattering. In those areas where conditions of specular reflections are fulfilled, short waves reduce the reflection coefficient (by a factor $1 - 4k_r^2 h_s^2$). Large-scale waves (carrying small-scale waves) cause random changes in the local incidence angle (affecting Bragg scattering) and may also provide the conditions for specular reflection.

The real waves are waves of the small slope. As it was argued in [11] tilting of the large-scale surface mainly results in small variations of local incidence angle $\tilde{\theta} \approx \eta_i$ (η_i is the surface slope in the plane of incidence). Neglecting the effect of tilting out of the incidence plane (see also Fig.5 in [7]) the averaged effect of large-scale waves on resonant scattering is

$$\sigma_{br}^p = \int_\Gamma \sigma_{0br}^p(\theta - \eta_i) P(\eta_i) d\eta_i \qquad (2)$$

where $\sigma_{0br}^p(\theta - \eta_i)$ is the Bragg NRCS (see e.g.[11]), $P(\eta_i)$ is the PDF of the large-scale surface slope in the direction of the incidence plane. In eq.(2) integral range Γ is defined as

$$\Gamma = \{\eta_i \le \mathrm{tg}(\theta - d/2) \cup \eta_i \ge \mathrm{tg}(\theta + d/2)\}$$

and results from the condition that local Bragg wave number must not exceed k_d. Note that if $\theta > 25^0 - 30^0$ the integral can be evaluated approximately by expansion of σ_{0br}^p in Taylor series up to the second order in the slope of tilting waves (e.g. [12, 7]). However at smaller θ (related to near range of SAR images) such expansion loses its validity.

It is suggested that on some of the large-scale surface patches (where $\eta_i \notin \Gamma$) conditions of the specular reflection can be fulfilled. Then these patches contribute to the NRCS by means of the specular reflection (second term in (1)). Expression for σ_{sp} can be found in e.g. [14, 13].

In [7] spectrum of the sea surface is defined as a composition of the wave spectrum of energy containing waves B_p and equilibrium spectrum B_{eq}:

$$B(\mathbf{k}) = B_p(\mathbf{k}) + B_{eq}(\mathbf{k}) \qquad (3)$$

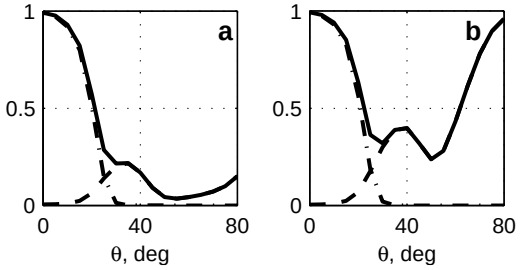

Fig.1. Relative contribution of quasi-specular reflection (dashed-dotted lines), wave breaking (dashed lines) and their sum (solid lines) to the total NRCS for VV (a) and HH (b) polarization at wind speed 10 m/s.

B_p in (3) is defined according to [3] , and shape of B_{eq} results from solution of the energy balance equation. In particular, in the equilibrium gravity range the energy balance presumes proportionality between energy input from wind and energy dissipation due to breaking of waves, i.e.

$$\beta \omega E(\mathbf{k}) \propto g^{-1} c^5 \Lambda(\mathbf{k}), \qquad (4)$$

where β is the wind growth rate, E is wave energy spectral density; c is phase speed; g is gravity acceleration; $\Lambda(\mathbf{k})$ is the surface density of the total length of breaking fronts of waves in the spectral interval from $\mathbf{k}$ to $\mathbf{k} + d\mathbf{k}$ introduced in [10]. The advantage of this wave breaking statistics is that the same $\Lambda(\mathbf{k})$-function defines both the energy dissipation (r.h.s. in (4)) and the fraction (q) of the sea surface covered by breaking waves:

$$\begin{aligned} q &\propto \int_{\mathbf{k} < \mathbf{k}_{wb}} k^{-1} \Lambda(\mathbf{k}) d\mathbf{k} \\ &= c_q \int_\phi \int_{k < k_{wb}} r_D \beta(\mathbf{k}) B(\mathbf{k}) d\varphi d \ln k \end{aligned} \qquad (5)$$

where $k_{wb} \approx 10 k_r$ is a wavenumber of shortest breaking waves providing radiowave scattering, r_D is the ratio of dissipation to wind input, c_q is a constant. To obtain the second relation in (5), we use (4).

An extensive comparison of the background NRCS model with observations at moderate θ is given in [7]. The most important results relate to polarization ratio, which at moderate θ is always less than the Bragg theory predictions. This fact was mentioned in many studies and clearly indicates that effects of wave breaking on radar scattering are significant. Model calculations done in [7] on total model (1) agree with observations, suggesting that the impact of wave breaking on NRCS is properly taken into account.

The relative contribution of breaking waves, specular reflections and their sum (so called non-Bragg scattering) to the total NRCS for C-band at VV and HH polarization and at wind speed 10 m/s is shown in Figure 1. Since σ_{wb} and σ_{sp} are independent of polarization and $\sigma_{br}^{V} > \sigma_{br}^{H}$, the relative contribution of non-Bragg scattering on HH polarization is higher than on VV one. At small incidence angle ($\theta < 20^0$) quasi-specular reflections dominate the NRCS both at HH and VV polarization. At HH polarization and moderate θ wave breaking contributes sufficiently to the NRCS while at large θ, it accounts for nearly the entire radar return. At VV polarization the role of wave breaking is quite different; at $\theta > 45^0$ its impact is negligible. This Figure can be used to assess the role of different informative parameters in the formation of radar signatures at C-band. At small θ variation in the mean square slope is the determining parameter. The role of Bragg waves and tilting waves is important at moderate θ for both polarizations. At HH polarization, wave breaking becomes important at moderate and dominates at large incidence angles. At VV polarization the role of wave breaking may be noticeable at $\theta \approx 25^0...45^0$ and is weak at larger incidence angle.

3. TRANSFORMATION OF WIND WAVES

Radar manifestations of oceanographic phenomena can result from modulation of the Bragg wave spectrum, mean square slope variations, and wave breaking in a non-uniform medium. We suggest that the major sources of medium non-uniformity are surface currents, wind field variations, and surfactants.

The characteristic form of the wave action spectral density $N(\mathbf{k})$ equation reads

$$\dot{N}(\mathbf{k},\mathbf{x},t) = Q\,;\ \dot{\mathbf{k}} = -\Omega_{\mathbf{x}}\,;\ \dot{\mathbf{x}} = \Omega_{\mathbf{k}} \qquad (6)$$

where dot means total derivative on time, low subscript means partial derivative, Q is the source of wave action spectral density. Also $\Omega = \omega(k) + \mathbf{k}\cdot\mathbf{u}$ is the frequency of waves in the moving medium: $\mathbf{u}$ is the surface current velocity; and ω is the intrinsic frequency. The background spectrum $N_0(\mathbf{k})$ results from solution: $Q(N_0) = 0$. Thus medium non-uniformities disturb the wind wave spectrum relative to its background shape.

3.1 Relaxation approximation

If the source Q is known, (6) with (7) can be solved numerically. However, in our model Q is defined in the equilibrium range only. In the range of energy containing waves, the saturation spectrum B_p is defined empirically. Therefore we analyze eqs. (6) following the relaxation approach developed in [9].

We assume that the energy source in (6) is a difference of wind energy input and a non-linear term: $\beta\omega N - Q_N$ The latter models energy dissipation due to wave breaking (D) and resonant wave-wave interactions (I): $Q_N = D + I$. Eq. (6) for small disturbances $\tilde{N}$ reads:

$$\dot{\tilde{N}} = \tilde{\beta}\omega N_0 - \tilde{N}/\tau \qquad (7)$$

$$\tau^{-1} = -\beta\omega + \partial Q_N / \partial N \qquad (8)$$

where τ is a relaxation time, which must be consistent with the energy source Q. Following [9] we suggest that eq. (7) must describe spectral variations caused by either currents or wind. Then the definition of τ is:

$$\omega\tau = \frac{m_*}{2\beta} \qquad (9)$$

where $m_* = \partial(\ln N_0)/\partial \ln u_*$ is the wind exponent of the wave spectrum. Such a definition of τ does not require any exact form of Q and one needs to know only exponent of the spectrum, which may be known e.g. empirically. For spectrum (3) the wind exponent is

$$m_* = (m_*^p B_p + m_*^{eq} B_e)/B \qquad (10)$$

According to [7], the wind exponent in the equilibrium range is $m_*^{eq} = 2/n$, where n is a function of k. It is equal to $n = 1$ in capillary-gravity range and $n = 5$ in the gravity range. The wind exponent for empirical spectrum B_p [3] at given fetch is $m_*^p = 1$ for developed sea, and $m_*^p \approx 0.7$ for developing one. This indicates that in a developed sea, the dominant role in Q_N comes from resonant wave-wave interactions (which are cubic in the action spectrum) and in the young sea both wave-wave interactions and wave breaking are important. Solution of eqs. (6) and (8) can be simplified for the following two asymptotic regimes. The first is when relaxation time τ is much less than scale L of medium non-uniformity, i.e. $\tau c_g / L$ is small (rapid relaxation

regime). The second asymptotic regime is when group velocity c_g is much larger than the current velocity scale $\hat{u}$, i.e. when $c_g/\hat{u}$ is large (fast wave regime).

We suggest that surface current and wind velocity may be expanded into the Fourier series. Then solution of eq. (6) in terms of amplitude of Fourier harmonic for wave spectrum variations $\hat{B}(\mathbf{k})$ reads

$$T(\mathbf{k},\mathbf{K}) = m_k^{ij}\hat{u}_{i,j}\frac{l_r}{c_g}\frac{1-i\cdot r}{1+r^2} - m_*\frac{\hat{u}_*}{u_*}\frac{r^2+ir}{1+r^2} \quad (12)$$

where $m_k^{ij} = k_j\partial \ln N/\partial \ln k_i$ is a tensor of "wavenumber exponent", $\hat{u}_{i,j}$ and $\hat{u}_*$ are Fourier harmonics for the tensor of current velocity gradient and variation of friction velocity in respect to the local value; $T = \hat{B}(\mathbf{k})/B_0(\mathbf{k})$ is modulation transfer function, $r = \mathbf{l}_\tau\cdot\mathbf{K} - \Omega\tau$ is dimensionless relaxation parameter, $\mathbf{l_r} = \mathbf{c_g}\tau$ is the relaxation scale, $\mathbf{K}$ is wavenumber of Fourier harmonic; $\Omega = C/K$; and C is its velocity of advance. Thus the saturation spectrum in physical space is

$$B(\mathbf{k},t) = B_0(\mathbf{k},t)\left[1 + \int T(\mathbf{k},\mathbf{K})e^{i(\mathbf{K}\cdot\mathbf{x}-\Omega t)}d\mathbf{K}\right] \quad (13)$$

Notice that eq.(12) includes also case of modulation of wind waves by long surface wave considered in [8].

For a given surface wave spectrum, calculations of the mean square slope in non-uniform medium are evident. To obtain relation for wave breaking modulations we suggest that in the energy containing range the exponent of energy dissipation dependence on the spectrum should be the same as in the equilibrium range, i.e. $n+1$=6 (see equation (16) in [7]). Then the harmonic Fourier of q modulation is

$$\hat{q}(\mathbf{K}) = c_q(n+1)\iint_{k<k_t} r_D\beta B(\mathbf{k})T(\mathbf{k},\mathbf{K})d\varphi d\ln k \quad (14)$$

It can be shown using the relaxation approach that the ratio of energy dissipation to wind input r_D is related to spectral wind exponent by

$$r_D = 2/3\cdot(m_*^{-1} - 1) \quad (15)$$

In the equilibrium range $m_* = 2/n = 2/5$, thus $r_D = 1$, i.e. wave breaking is a dominating non-linear term. In the energy containing range and a developed sea $r_D = 0$, i.e. wave breaking dissipation is negligible. For a young sea ($m_* = 0.7$) the contribution of wave breaking to the energy balance is $r_D \approx 0.3$.

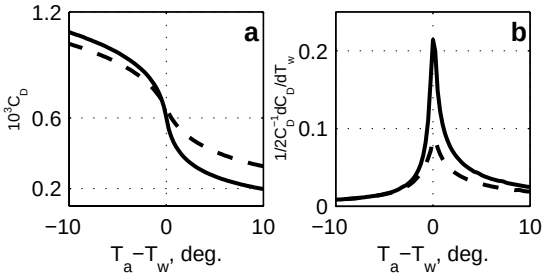

Fig.2. a) Geostrophic drag coefficient as a function of the temperature drop between the sea surface and free atmosphere for geostrophic wind speed 5 m/s (solid lines) and 15 m/s (dashed line). b) Transfer function $1/2\partial(\ln C_D)/\partial T_W$ describing linear response of air friction velocity on the surface temperature variations.

4. IMPACT OF MABL

In many cases ocean phenomena are accompanied with spatial variations of the surface temperature T_w (temperature fronts). Changes in T_w affect stratification of the marine atmospheric boundary layer (MABL) and thus wind surface stress and wind waves. Experimental evidence on correlation of radar return and T_w is given in [1]. To assess effect of MABL we assume that geostrophic wind speed G and temperature of the free atmosphere T_a are horizontally uniform. Then any variations in the surface wind are the result of the planetary MABL transformation over varying T_w. We suggest that wind surface stress may be estimated through the resistance law for the equilibrium planetary MABL, which reads (e.g. [2])

$$\frac{\kappa\mathbf{G}}{\mathbf{u}_*} = \ln(\kappa u_*/fz_0) - B(\mu) - iA(\mu) \quad (16)$$

where $\mu = \kappa u_*/fL$ is the MABL stratification parameter, L is the Monin-Obukhov scale; f is Coriolis parameter, $\mathbf{G} = G\exp(i\varphi_G)$ is complex geostrophic wind velocity; φ_G is its direction; $\mathbf{u}_* = u_*\exp(i\varphi_w)$ is complex friction velocity, φ_w is direction of the near surface wind; z_0 is the sea surface roughness scale. The universal functions $A(\mu)$ and $B(\mu)$ are defined according to [2]. Geostrophic drag coefficient $C_D = u_*^2/G^2$ as a function of $T_a - T_w$ is shown in panel a of Fig. 2 for G = 5 m/s and G=15 m/s. If we suggest that on the upwind side of the front

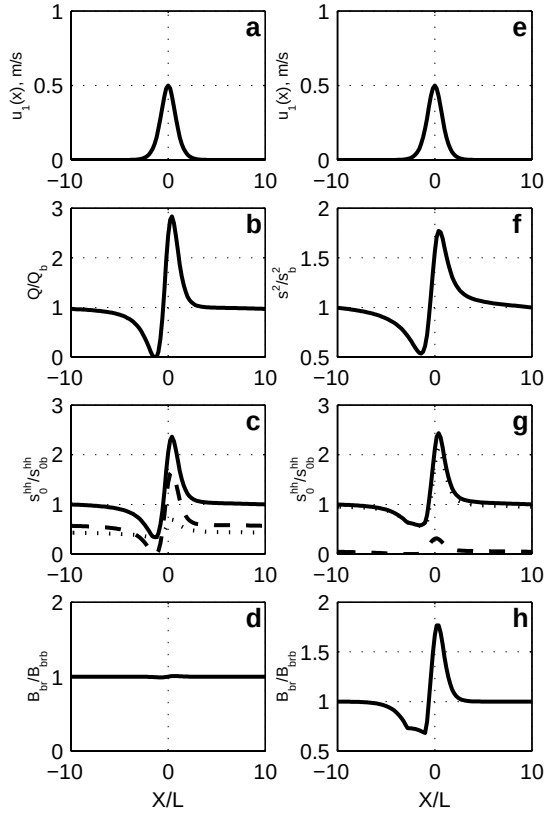

Fig.3. Model calculations of the sea surface manifestation of internal waves traveling upwind.
a,e) Current velocity induced by IW on the sea surface.
b) Modulation of wave breaking.
c) Modulation of the sea surface NRCS at X-band HH polarization: solid line is total NRCS, wave breaking component is dashed line, and Bragg scattering component is dotted line. Contribution of specular component is negligible.
d) Modulation of X-band Bragg waves.
f) Modulation of mean square slope.
g) The same as in c) but for L-band.
h) Modulation of L-band Bragg waves.

MABL stratification is neutral ($T_a - T_w$=0) and the air flow is running on the warm/cold front with the surface temperature drop $|\Delta T_w| = 5^0$, surface wind stress on the downwind side is increased/decreased in 1.7 times. Such enhancement/suppression of wind stress may cause essential variations in wind waves resulting in radar manifestation of a sea front. A linear response of u_* on the surface temperature variations $\widetilde{T}_w$ $\widetilde{u}_* / u_* = [1/2\partial(\ln C_D)/\partial T_w]\widetilde{T}_w$ is shown in panel b of Fig.2. Response of friction velocity is strongest when variations in T_w occur on the background of neutral MABL, and weak if background stratification is either stable or unstable.

5. COMPARISON WITH EXPERIMENTS

5.1 Internal Waves

First we consider radar signatures of internal waves (IW) as the most reliable way to check the model. We chose well-controlled experiment SARSEX [4]. During this experiment trains of soliton-like IW have been observed. Here we model radar signatures of IW packet G. Scale of phase speed of these IW and amplitude of surface velocity were C=0.7 m/s and u_0=0.5 m/s, correspondingly. Wind speed was 6.0 m/s and its direction in respect to direction of the IW traveling was θ_w= -145^0 (i.e. IWs travel approximately opposite to the wind direction). Airborne X- and L-band SAR images on HH polarization of this IW packet can be found in [4]. Radar signature of range travelling IW were observed at incidence angle θ=35^0 -45^0.

Results of the model simulation are presented in Fig. 3. As mentioned previously, both wave breaking and mean square slope are significantly disturbed by the IW, with the amplitude of q modulation exceeding the one from s^2 by a factor of two. Enhancement of wave breaking is shifted to the forward face of IW, i.e. toward the region of maximum convergence of the surface current. Peak-over-background ratio for X- and L-band is approximately the same and equal to 2.5 (or 4 dB). These estimates are consistent with radar observations. As it follows from Fig.3 the physics responsible for the enhanced radar return in X- and L-band is different. In X-band peak of radar modulation results from scattering from enhanced breaking waves (65%) and Bragg

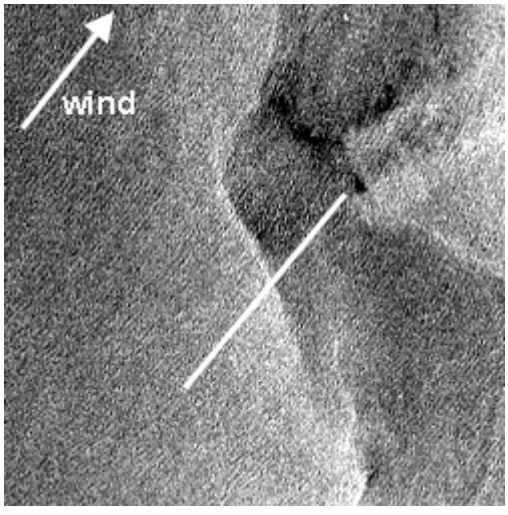

Fig. 4. Extract (30x30 km) of ERS-2 SAR image of Norwegian coastal current obtained at 10:31 on 27 September 1995. Arrow indicates wind direction. White line is the ship route where measurements shown in Fig. 5 were done.

scattering mechanism contributes 35% of return power by means of modulation of mean square slope of tilting waves (in X-band modulation of Bragg waves in negligible). In L-band modulation of Bragg scattering mechanism is a primary source of radar scattering modulations. In this case both modulation of Bragg waves (see plot h) and slope of tilting waves are of the same importance. One may mention that X-band and L-band signatures of the same IW exhibit similar modulation patterns. This experimental fact was mentioned in all studies on radar signatures of IW.

5.2 Sea front: CoastWatch-95 experiment

During the "CoastWatch-95" experiment 56 ERS-1/2 SAR images of the Norwegian coastal zone and *in situ* data (meteorological parameters, surface current velocity, sea temperature and salinity in the upper layer) were collected [6]. In this paper we analyze SAR image obtained at 10:31 on 27.09.1995, when the time gap between the SAR image and *in situ* measurements taken from the ship travelling across the front was minimal, 21 minutes. An extract of the SAR image is shown in Fig. 4. *In situ* measurements along the ship track (indicated on SAR image) are presented in Fig. 5. The drop of T_w across the front is about 4°. In general surface current has a form of a jet-like current running along the front. However in the vicinity of the front it has a perpendicular to the front component. The air-water temperature difference has the opposite sign on the cold and warm sector of the front. This means that the MABL stratification is unstable in the warm sector and stable in the cold one. During the ship measurements, the air flow was steady in direction while its mean wind speed was around 9.5 m/s. Section of the SAR image along ship route shown in Fig. 4 is presented in Fig. 6a. The most remarkable features of the SAR images are easy recognizable. They are: the higher radar scattering from the warm side of the front, and enhanced radar returns in the vicinity of the sea surface temperature front.

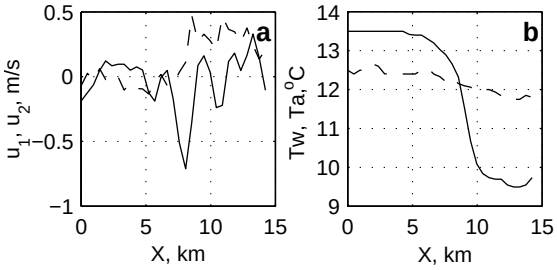

Fig. 5. Measurements taken from the ship crossing the sea front along the line shown in SAR image, Fig. 4.
a) Components of the current velocity parallel (dashed line) and perpendicular (solid line) to the front. b) The sea surface temperature (solid line) and air temperature (dashed line) at $z = 15$ m

Measurements of the sea surface and air temperature, and current velocities shown in Fig. 5 were used to simulate the NRCS of the sea surface. On the first step we have calculated transformation of wind surface stress over the front with use of resistance law (16). Then varying friction velocity and surface currents were used as input for the wind waves transformation equations (12), (13) and (14). These calculations (not shown) indicated that decrease of the wind stress on the cold side of the front causes decrease of the mean square slope and wave breaking. Surface current gives additional contribution to wave transformation. Effect of the current on wave breaking is much stronger than on the mean slope, and wave breaking (as well as MSS) following divergence of the surface current. Effect of the current shear is negligible. Model and observed

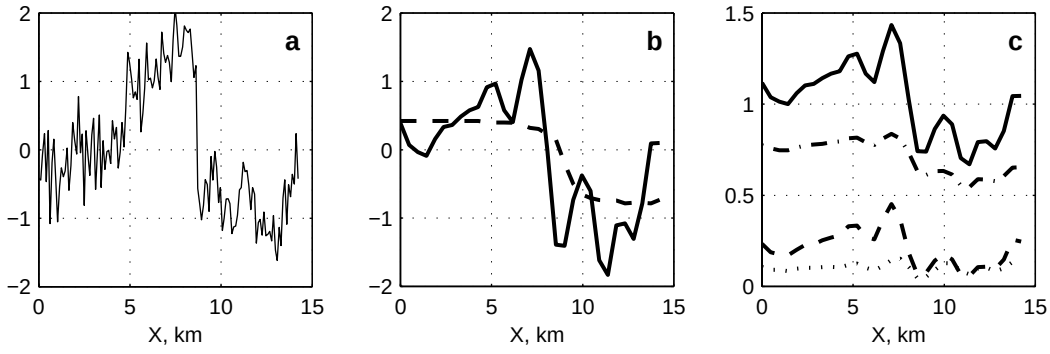

Fig. 6. a) Section of the SAR images (normalized on mean value, in dB) along the line shown in Fig. 4. b) Model NRCS over the front (normalized on mean value in dB), Dashed line demonstrates pure effect of MABL stratification. Solid line is the total NRCS variations caused by current and MABL. c) Relative contribution of different scattering mechanism (normalized on mean NRCS, linear scale): Solid line is total NRCS; dashed-dotted line is contribution of Bragg scattering; dashed line is contribution of wave breaking; dotted line is contribution of specular reflection

radar signatures of the front for the geometry of SAR observations ($\theta = 23^0$ and radar look direction in respect to frontal line is $\varphi = 135^0$) are shown in Fig. 6. The dashed line in Fig. 6b demonstrates effect of MABL stratification resulting in the stronger radar scattering on the warm side of the front. Solid line shows joint atmospheric and current effect. Fig. 6c demonstrates impact of varying scattering mechanisms on radar return. As it follows from this plot, on the upwind side of the front Bragg scattering is dominating mechanism providing about 80% of the radar return power. However in the vicinity of the front, wave breaking is enhanced. This process causes a significant increase in the radar return. Comparing the contribution of different scattering mechanisms one may conclude that maximum of radar return in the vicinity of the front results from enhanced wave breaking. Effect of the current on radar return mainly follows its divergence. One may conclude that the shapes of observed and model section of the SAR image over the front are quite similar.

6. CONCLUSION

We proposed a radar imaging model of oceanic phenomenon of the arbitrary origin. This model is the extension of semi-empirical model of the sea surface NRCS developed in [7] on the case of the non-uniform medium. It takes into account scattering from "regular" surface (due to Bragg scattering and specular reflections) and scattering from breaking waves. The same wave breaking statistics proposed in [10] is consistently used in the electromagnetic and hydrodynamic component of the radar imaging model.

Wave breaking may significantly contribute to the NRCS at moderate and large incidence angles. At small angles, specular scattering from "regular" (non-breaking) regions of the surface is another important non-Bragg scattering mechanism. Non-Bragg scattering is independent of polarization. Hence its relative role at HH polarization is higher than at VV. At L-band, the impact of non-Bragg scattering is negligible, while at C-band (and at higher radar frequencies) non-Bragg scattering plays an important role.

Transformation of wind waves is described in relaxation approximation. In this model, the relaxation parameter is related to the form of the source term, and hence gives consistency between the background sea state and its transformation in non-uniform media. Surface currents, variable near-surface wind fields (resulting from MABL transformations over surface temperature fronts), and surfactants are considered as the main sources of the medium non-uniformity. Application of the NRCS model to radar MTF is given in [8]. In the present paper we compared the model with experimental data obtained in SARSEX and CoastWatch95 experiments. A reasonably good agreement between model and observations is obtained.

Acknowledgements:

The authors acknowledge the support of INTAS Association under the Project INTAS-00-598 and the support from the Norwegian Space Center. D. Akimov acknowledges support from INTAS under Young Scientist grant #2002-419.

REFERENCES

1. Beal, R., V. Kudryavtsev, D. Thompson, S. Grodsky, D. Tilley, V. Dulov, and H. Graber, The influence of the marine atmospheric boundary layer on ERS-1 synthetic aperture radar imagery of the Gulf Stream, *J. Geophys. Res.*, 102, C3, 5799-5814, 1997.

2. Brown, R.A., On two-layer models and the similarity functions for the PBL, *Bound. Layer Meteor.*, 24, 451-463, 1982.

3. Donelan, M.A., J.Hamilton, and W.H. Hui, Directional of wind generated waves, *Philos. Trans. R. Soc. London*, Ser.A, 315, 509-562, 1985.

4. Gasparovich R.F., J.A. Apel, and E.S. Kasischke, An overview of the SAR internal wave signature experiment, *J. Geophys. Res.,* 93, C10, 12,304- 12,316, 1988.

5. Johannessen, J., R. Shuchman, G. Digranes, D. Lyzenga, W. Wackerman, O. Johannessen, and P. Vachon, Coastal ocean fronts and eddies imaged with ERS-1 synthetic aperture radar, *J. Geophys. Res.*, 101, 6651-6667, 1996.

6. Johannessen, O.M., E. Korsbakken, P. Samuel, A.D. Jenkins and H. Espedal, COAST WATCH: Using SAR imagery in an operational system for monitoring coastal currents, wind, surfactants and oil spills. In *Operational Oceanography. The Challenge for European Co-operation*. J.H. Stel (editor-in-chief), Elsevier Oceanography Series, 62, 1997.

7. Kudryavtsev, V., D. Hauser, G. Caudal, and B. Chapron, A semi-empirical model of the normalized radar cross-section of the sea surface. Part 1: The background model, *J. Geophys. Res*., 108, C3, DOI 10.1029/2001JC001003, 2003.

8. Kudryavtsev, V., D. Hauser, G. Caudal, and B. Chapron, A semi-empirical model of the normalized radar cross-section of the sea surface. Part 2: Radar modulation transfer function, *J. Geophys. Res*., 108, C3, DOI 10.1029/2001JC001004, 2003.

9. Kudryavtsev, V., The coupling of wind and internal waves: modulation and friction mechanism*, J.Fluid Mech*., 278, 33-62, 1994.

10. Phillips, O. M., Spectral and statistical properties of the equilibrium range in the wind-generated gravity waves, *J.Fluid Mech*., 156, 505-531, 1985.

11. Plant, W.J., Bragg scattering of electromagnetic waves from the air/sea interface, in Surface *Waves and Fluxes, Volume II - Remote Sensing*, 41-108, 1990.

12. Romeiser R., and W.Alpers, An improved composite surface model for the radar backscattering cross section of the ocean surface. 2. Model response to surface roughness variations and the radar imaging of uderwater bottom topography, *J. Geophys. Res.*, 102, C11, 25,251-25,267, 1997.

13. Thomson, D.R., Calculation of radar backscatter modulations from internal waves, *J. Geophys. Res*., 93, C10, 12,371-12,380, 1988.

14. Valenzuela, G.R., M.B.Laing, and J.C.Daley, Ocean spectra for the high frequency waves as determined from airborne radar measurements, *J. Marine Res.*, 29, №.2, 69-84, 1971.